J. Fluid Mech. (1997), *vol.* 345, *pp.* 79–99. Printed in the United Kingdom

Stochastic nonlinear shoaling of directional spectra

By Y. AGNON[1]† AND A. SHEREMET[2]

[1]Department of Civil Engineering, Technion, Haifa 32000, Israel

[2]CAMERI – Coastal and Marine Engineering Research Institute, Technion City, Haifa 32000, Israel

(Received 17 May 1996 and in revised form 19 March 1997)

We derive a deterministic directional shoaling model and a stochastic directional shoaling model for a gravity surface wave field, valid for a beach with parallel depth contours accounting for refraction and nonlinear quadratic (three wave) interactions. A new phenomenon of non-resonant spectral evolution arises due to the medium inhomogeneity. The kernels of the kinetic equation depend on the bathymetry through an integral operator. Preliminary tests carried out on laboratory data for a unidirectional case indicate that the stochastic model also works rather well beyond the region where the waves may be regarded as nearly Gaussian. The limit of its applicability is decided by the dispersivity of the medium (relative to the nonlinearity). Good agreement with both laboratory data and the underlying deterministic model is found up to a value of about 1.5 for the spectral peak Ursell number. Beyond that only the deterministic model matches the measurements.

1. Introduction

Much of the work devoted in recent years to the study of shoaling wave fields has been directed at the more tractable simplifications of the problem assuming unidirectionality, a mild bottom slope and weak dispersion. For the shallow-water case one may cite the extensively tested Boussinesq-type model developed by Freilich & Guza (1984), having quadratic near-resonant interactions as the dominant energy exchange mechanism. The angular spectrum model derived by Suh, Dalrymple & Kirby (1990) falls in the class of Schrödinger-type models, valid at the deeper end of the beach, for a narrow spectrum and a dominant cubic-interaction nonlinear energy exchange mechanism. The implied assumption of weak dispersion in the above models is dropped in the work of Agnon *et al.* (1993). The evolution equation derived describes the shoaling of unidirectional arbitrary wide spectra all the way from deep into shallow water, with no restriction on the dispersion of the waves. They assumed that refraction and the dominant nonlinear triad interactions are of the same order and neglected cubic and higher-order processes.

The degree of complexity of a model may be increased further by widening its scope to include directional spread, breaking, mean flows – a plethora of processes may be brought in. A deterministic model such as the ones mentioned has, however, limited utility. The sea state is essentially a stochastic process, and so in order to

† Present address: Centre for Computational Hydrodynamics (ICCH), Danish Hydraulic Institute, Agern Alle 5, DK-2970 Hørsholm, Denmark.

obtain a viable wave forecast one has to run the model over and over again, on many different initial data sets and average the results. Apart from the question of how many such data sets one needs, deep-water wave forecasts and measured data come usually in the form of power spectra estimates with no information about modal phases. Additional arbitrary assumptions about the missing data are then made – usually uniformly distributed random phases. The alternative, which we pursue here, is a stochastic shoaling model.

Regarding the system as stochastic, one seeks to describe its evolution by deriving a hierarchy of equations for the statistical moments, or equivalently the Fourier space cumulants. This approach leads to the well-known closure problem fundamental to nonlinear processes: the evolution equation for a moment of a given order depends on the moments of higher orders, and without additional assumptions one is left with an infinite set of equations to solve. This is the classical problem of closure.

In the case of a weakly nonlinear system such as water waves, one way to derive some information from these equations is to use assumptions that discard all the cumulants of order higher than a specified value: the Gaussian approximation, for example, amounts to neglecting cumulants higher than the second. Now, even if the waves are Gaussian at one location, the evolution equation for the third-order moment contains a fourth-order moment and a product of second-order moments (see Benney & Newell 1969), and so the third-order one should not be expected to remain zero. The shoaling processes in particular are characterized by a very fast evolution, in the range of at most a few tens of wavelengths, as the system evolves from dominant cubic to dominant quadratic near-resonant nonlinear interactions (a more intensive energy exchange mechanism) and from a dispersive to a weakly dispersive medium. As a result the shallow-water waves exhibit very strongly phase-coupled Fourier modes and may by no means be regarded as Gaussian.

The first in a sequence of asymptotic closures for weakly nonlinear systems was obtained by Benney & Saffman (1966), who were able to show that earlier results based upon cumulant discarding assumptions were valid without the necessity of making any restrictive assumptions. In a subsequent series of papers, Benney & Newell (1969) and Newell & Aucoin (1971) among others extended the original derivations to higher-order closures and discussed further several specific systems. They describe the mechanism that enables the closure as the action of two separate processes. The first occurs on a time (length) scale given by a characteristic period (wavelength) of the waves involving the decoupling of the initial correlations due to the dispersive nature of the waves, and an approach to the Gaussian state as one might expect from the Central Limit Theorem. The second process, occurring over longer scales, given by the characteristic nonlinear time (length) scale, is one of regeneration of these higher cumulants by nonlinear coupling. The dispersive nature of the medium is essential. Newell & Aucoin (1971) coined the phrase 'semi-dispersive' to denote non-dispersive media with more than one dimension; closure may still be obtained here with some quite fine tuning of the theory, due to the dispersive effect of waves travelling in different directions (these ideas appear in the stochastic directional shallow water model developed by Abreu, Larazza & Thornton 1992). In one-dimensional non-dispersive media there is no substitute for dispersion that can induce the decay of the initial correlations, which are conserved and enhanced by the nonlinearity, and no such closure seems possible.

In §2 we discuss the general restrictions imposed on the present model and make some preparatory manipulations of the original governing equations. In the absence of edge waves, the evolution equation derived by Agnon *et al.* (1993) is readily

generalized to a nonlinear second-order shoaling one valid for obliquely incident and directionally spread spectra, over a mildly sloped bottom. The extension to the directional deterministic shoaling model is straightforward and we give only its final form. Starting from this equation, the present study derives, under the restriction of parallel depth contours, a stochastic directional shoaling model that accounts for nearly resonant quadratic interactions, presented in §3.

The shoaling problem is one of an inhomogeneous medium. As the waves shoal, the locked, or bound, waves increase in magnitude, while the dispersion decreases. The kinetic equation for the energy spectrum has to account for the phase correlation structure, which is reflected in the bispectrum, or in the distribution of the wave motion at any frequency among the free waves and the locked waves at different wavenumbers. We need an equation that has a 'memory', and indeed we obtain such an equation. The kernels of the equation depend on the variation of the wavenumbers which depend on the variation of the bottom depth. It is well known that in deep water, or in water of constant depth, spectral evolution requires exact resonant conditions (which cannot be satisfied by triads of gravity waves). In contrast, the kernels obtained for shoaling waves have the form of 'smeared delta functions' and account for the important process of non-resonant triad interactions.

Section 4 presents experimental testing of the present model and comments on its utility compared with the original deterministic one. The stochastic model appears to be superior in several respects to the deterministic one, but further testing is needed. Conclusions are given in §5.

2. Formulation of the problem

We write the equations governing the irrotational flow of an inviscid fluid with a free surface, after expanding the surface boundary conditions in power series about $z = 0$ and discarding all terms higher than quadratic in the wave steepness ϵ, where $\epsilon \ll 1$. They are the Laplace equation:

$$\nabla^2\phi + \phi_{zz} = 0, \quad -h \leqslant z \leqslant 0, \tag{2.1}$$

the bottom boundary condition:

$$\phi_z + \nabla h \cdot \nabla\phi = 0, \quad z = -h, \tag{2.2}$$

the free-surface kinematic boundary condition:

$$\eta_t - \phi_z + \nabla \cdot (\eta\nabla\phi) = 0, \quad z = 0, \tag{2.3}$$

and the free-surface dynamic boundary condition:

$$\phi_t + g\eta + \eta\phi_{tz} + \tfrac{1}{2}|\nabla\phi|^2 + \tfrac{1}{2}(\phi_z)^2 = 0, \quad z = 0, \tag{2.4}$$

where ∇ is the horizontal gradient and ϕ, η and h are the velocity potential, the free-surface displacement and the local water depth, respectively. The origin of the reference frame is taken in deep water at the still water level, with the z-axis upwards. By eliminating η from (2.3)–(2.4) a new form of the system of governing equations may be obtained:

$$\nabla^2\phi + \phi_{zz} = 0, \quad -h \leqslant z \leqslant 0, \tag{2.5}$$

$$\phi_z + \nabla h \cdot \nabla\phi = 0, \quad z = -h, \tag{2.6}$$

$$\phi_{tt} + g\phi_z = \left[-\tfrac{1}{2}|\nabla\phi|^2 - \tfrac{1}{2}(\phi_z)^2 + \frac{1}{g}\phi_t\phi_{zt}\right]_t - \nabla \cdot (\phi_t\nabla\phi), \quad z = 0, \tag{2.7}$$

$$g\eta = -\phi_t + \frac{1}{g}\phi_t\phi_{zt} - \tfrac{1}{2}|\nabla\phi|^2 - \tfrac{1}{2}(\phi_z)^2, \quad z = 0, \tag{2.8}$$

where the first three equations form a closed system for ϕ, and η is given as a function of ϕ via (2.8).

In what follows we make no assumptions regarding the shallowness of the water, which is to say kh may be $O(1)$, with k the characteristic wavenumber, so that the linear dispersion relation has to be used in its full form; we do assume that the beach slope is mild, that is $|\nabla h| = O(\epsilon)$ or smaller.

Next, we shall use a multiple scale approach, by defining the slow time $t_1 = \epsilon t$ with the time derivative written accordingly as $\partial_t \to \partial_t + \epsilon\partial_{t_1}$, expand (2.5)–(2.8) and retain, for consistency, only terms up to $O(\epsilon^2)$ with respect to the leading terms.

The velocity potential and the free-surface displacement will be expressed as

$$\phi = \phi_0(x, y, t_1) + \epsilon\phi_1(x, y, z, t, t_1), \tag{2.9}$$

$$\eta = \epsilon\eta_0(x, y, t_1) + \epsilon\eta_1(x, y, t, t_1). \tag{2.10}$$

Here ϕ_1 and η_1 refer to the wave movement, and ϕ_0, η_0 denote the slowly varying mean flow and set-down induced by the waves. It is assumed that $\nabla\phi_0$ and $\nabla\eta_0$ are $O(\epsilon)$. The drift velocity potential is formally allowed to be of first order to account for the growth of the current from $O(\epsilon^2)$ in deep water to the same order as the orbital velocity in shallow water.

In order to separate two systems of equations, one for the slowly varying ϕ_0 and η_0, the 'zero frequency' mode, and another for the fast components ϕ_1, η_1, it will be useful to eliminate the variable t by using the Fourier transform to go over to the frequency domain:

$$\hat{\phi}(\omega, t_1) = \int_{-\infty}^{\infty} \phi(t, t_1)\mathrm{e}^{-\mathrm{i}\omega t}\mathrm{d}t, \tag{2.11}$$

$$\phi(t, t_1) = \frac{1}{2\pi}\int_{-\infty}^{\infty} \hat{\phi}(\omega, t_1)\mathrm{e}^{\mathrm{i}\omega t}\mathrm{d}\omega. \tag{2.12}$$

After some algebra, which is similar to the derivation in Agnon *et al.* (1993), the governing equations (2.1)–(2.4) yield for the fast components the system

$$\nabla^2\hat{\phi}_1 + \hat{\phi}_{1zz} = 0, \quad -h \leqslant z \leqslant 0, \tag{2.13}$$

$$\hat{\phi}_{1z} + \nabla h\cdot\nabla\hat{\phi}_1 = 0, \quad z = -h, \tag{2.14}$$

$$\begin{aligned} -\omega^2\hat{\phi}_1 + g\hat{\phi}_{1_z} = {} & -2\mathrm{i}\omega\hat{\phi}_{1t_1} - \{2\mathrm{i}\omega\nabla\phi_0\cdot\nabla\hat{\phi}_1 + \eta_0[\omega^2\hat{\phi}_{1_z} - g\nabla^2\hat{\phi}_1]\} \\ & + \frac{\mathrm{i}\omega}{4\pi}\int_{-\infty}^{\infty}\left[\nabla\hat{\phi}_1^{(1)}\cdot\nabla\hat{\phi}_1^{(2)} + \hat{\phi}_{1z}^{(1)}\hat{\phi}_{1z}^{(2)} + 2\frac{\omega_1\omega_2}{g}\hat{\phi}_1^{(1)}\hat{\phi}_{1z}^{(2)}\right. \\ & \left. + 2\frac{\omega_1}{\omega}\nabla\cdot(\hat{\phi}_1^{(1)}\nabla\hat{\phi}_1^{(2)})\right]\delta(\omega - \omega_1 - \omega_2)\mathrm{d}\omega_1\mathrm{d}\omega_2 + O(\epsilon^3), \ z = 0, \end{aligned} \tag{2.15}$$

$$\begin{aligned} -g\hat{\eta}_1 = {} & \mathrm{i}\omega\hat{\phi}_1 + [\hat{\phi}_{1_{t_1}} + \mathrm{i}\omega\eta_0\hat{\phi}_{1_z} + \nabla\phi_0\cdot\nabla\hat{\phi}_1] \\ & + \frac{1}{4\pi}\int_{-\infty}^{\infty}\left[\nabla\hat{\phi}_1^{(1)}\cdot\nabla\hat{\phi}_1^{(2)} + \hat{\phi}_{1_z}^{(1)}\hat{\phi}_{1_z}^{(2)} + 2\frac{\omega_1\omega_2}{g}\hat{\phi}_1^{(1)}\hat{\phi}_{1_z}^{(2)}\right] \\ & \times\delta(\omega - \omega_1 - \omega_2)\mathrm{d}\omega_1\mathrm{d}\omega_2 + O(\epsilon^3), \quad z = 0, \end{aligned} \tag{2.16}$$

where the notation

$$\hat{\phi}_1^{(1)}\hat{\phi}_1^{(2)} = \hat{\phi}_1(x, y, z, \omega_1, t_1)\hat{\phi}_1(x, y, z, \omega_2, t_1) \tag{2.17}$$

was used in the integrands of (2.15)–(2.16). For the slowly varying components we shall prefer to use the surface boundary conditions in the form (2.3)–(2.4) and obtain

$$\left[\eta_{0t_1} + \nabla\cdot(h\nabla\phi_0)\right]\delta(\omega) = -\left[\nabla\cdot(\eta_0\nabla\phi_0)\right]\delta(\omega) + \frac{1}{4\pi^2}\int_{-\infty}^{\infty}\frac{\mathrm{i}\omega}{g}\nabla\cdot(\hat{\phi}_1\nabla\hat{\phi}_1^*)\mathrm{d}\omega + O(\epsilon^4), \quad z=0, \tag{2.18}$$

$$\left[\phi_{0t_1} + g\eta_0\right]\delta(\omega) = -\left[\tfrac{1}{2}(\nabla\phi_0)^2\right]\delta(\omega) - \frac{1}{8\pi^2}\int_{-\infty}^{\infty}\left[|\nabla\hat{\phi}_1|^2 + |\hat{\phi}_{1_z}|^2 - 2\frac{\omega^2}{g}\hat{\phi}_1(\hat{\phi}_{1_z})^*\right]\mathrm{d}\omega + O(\epsilon^3), \quad z=0. \tag{2.19}$$

The systems of equations (2.18)–(2.19) and (2.13)–(2.16) form the starting point for the derivation of the evolution equation for a directional gravity wave spectrum that will be presented in the following sections.

3. The stochastic evolution equation

The main task in the derivation of the evolution equation for a shoaling directional gravity wave spectrum is to reduce the three-dimensional system (2.13)–(2.16) to a single equation by eliminating the vertical structure of the function $\hat{\phi}_1$. Assuming that no significant edge-wave modes are generated, a directional shoaling model may be obtained as a straightforward generalization of the method used by Agnon *et al.* (1993) for the unidirectional case. We shall not present the derivation here (the details may be found in Sheremet 1996), but cite only several definitions that are used as a starting point in the derivation and are also needed in what follows. We look for a solution as a sum of a free and a locked wave forced by pairs of free waves (higher-order locked waves are not effective on the characteristic scales of the shoaling process). The velocity potential is written as:

$$\hat{\phi}_1 = \hat{\phi}_{1F} + \hat{\phi}_{1L} = \varphi_F Z_F + \frac{\epsilon}{\mu}\int_{-\infty}^{\infty}\varphi_L Z_L\delta(\omega-\omega_1-\omega_2)\mathrm{d}\omega_1\mathrm{d}\omega_2, \tag{3.1a}$$

$$\hat{\phi}_1|_{z=0} = \varphi = \varphi_F + \frac{\epsilon}{\mu}\int_{-\infty}^{\infty}\varphi_L\delta(\omega-\omega_1-\omega_2)\mathrm{d}\omega_1\mathrm{d}\omega_2, \tag{3.1b}$$

where the functions $Z_{F,L} = \cosh k_{F,L}(z+h)/\cosh(k_{F,L}h)$ are the free and locked waves vertical structure respectively, with $\boldsymbol{k}_L = \boldsymbol{k}_F(\omega_1) \pm \boldsymbol{k}_F(\omega_2)$ and $k_{F,L} = |\boldsymbol{k}_{F,L}|$.

The measure of the departure of the locked wave from the free wave character is given by the detuning parameter:

$$\mu = \frac{|\boldsymbol{k}_F(\omega) - (\boldsymbol{k}_F(\omega_1) \pm \boldsymbol{k}_F(\omega_2))|}{|\boldsymbol{k}_F(\omega)|}, \tag{3.2}$$

which evolves from $O(1)$ in deep water, where the locked wave is of second order with respect to the free wave, to $O(\epsilon)$ in shallow water as the system approaches quadratic resonance and the locked wave grows to the same order as the free wave. We have therefore taken it explicitly in (3.1) of order ϵ/μ. The absence of edge waves allows one to use a formal WKB expansion that leads (see the references cited above) to the evolution equation for the complex amplitude of φ:

$$\frac{\partial A}{\partial t_1} + \tfrac{1}{2}\nabla\cdot\boldsymbol{C}_g A + \boldsymbol{C}_g\cdot\nabla A + \mathrm{i}\left[\frac{g}{2\omega}(k^2-\sigma^4)\eta_0 + \boldsymbol{k}\cdot\nabla\phi_0\right]A$$
$$= \int_{-\infty}^{\infty} \boldsymbol{W}_{(0,1,2)} A_1 A_2 \exp\left[\mathrm{i}\int(\boldsymbol{k}-\boldsymbol{k}_1-\boldsymbol{k}_2)\mathrm{d}\boldsymbol{x}\right]\delta^{\omega}_{0:1,2}\mathrm{d}\omega_1\mathrm{d}\omega_2, \qquad (3.3a)$$

$$\boldsymbol{W}_{(0,1,2)} = \frac{1}{8\pi}\left(2\boldsymbol{k}_1\cdot\boldsymbol{k}_2 + (\sigma_1\sigma_2)^2 + k_1^2\frac{\sigma_2}{\sigma} + k_2^2\frac{\sigma_1}{\sigma} - \sigma^2\sigma_1\sigma_2\right), \qquad (3.3b)$$

$$\sigma_j^2 = \frac{\omega_j^2}{g} = k_j\tanh(k_j h) \qquad (3.3c)$$

where

$$\varphi = A\mathrm{e}^{-\mathrm{i}\int \boldsymbol{k}\mathrm{d}\boldsymbol{x}},$$

$\delta^{\omega}_{0:1,2}$ is shorthand for $\delta(\omega-\omega_1-\omega_2)$ and $\boldsymbol{C}_g = C_g\boldsymbol{k}/k$ is the vector group velocity. For the unidirectional case of waves propagating normally to the shore, this coincides with the result obtained by Agnon *et al.* (1993). When the depth variation in the direction parallel to the beach is much slower than the slope normal to the beach, the wavenumber in the long-shore direction is another constant of motion, in addition to the frequency. Going over to the long-shore wavenumber domain turns out to simplify considerably the description of directional spectra (the idea is described in detail in Suh *et al.* 1990). Denote the cross- and long-shore coordinates by x and y respectively, and the corresponding wavenumbers k_x and κ. Formally, taking the Fourier transform of the evolution equation over y amounts to bringing κ and ω onto an equal footing in (3.3), which gives

$$\frac{\partial A}{\partial t_1} + \frac{1}{2}\frac{\partial}{\partial x}\left(\frac{k_x}{k}C_g\right)A + C_g\frac{k_x}{k}\frac{\partial A}{\partial x} + \mathrm{i}\left[\frac{g}{2\omega}(k^2-\sigma^4)\eta_0 + k_x\phi_{0x}\right]A$$
$$= \int_{-\infty}^{\infty}\boldsymbol{W}_{(0,1,2)}A_1A_2\exp\left[-\mathrm{i}\int_{-\infty}^{x}(k-k_1-k_2)\mathrm{d}x\right]\delta^{\omega}_{0:1,2}\delta^{\kappa}_{0:1,2}\mathrm{d}\omega_1\mathrm{d}\omega_2\mathrm{d}\kappa_1\mathrm{d}\kappa_2 \qquad (3.4a)$$

$$\boldsymbol{W}_{(0,1,2)} = \frac{1}{8\pi}\left[2\boldsymbol{k}_1\cdot\boldsymbol{k}_2 + (\sigma_1\sigma_2)^2 + k_1^2\frac{\sigma_2}{\sigma} + k_2^2\frac{\sigma_1}{\sigma} - \sigma^2\sigma_1\sigma_2\right]. \qquad (3.4b)$$

The wavenumber squared is $k_i^2 = k_{x,i}^2 + \kappa_i^2$. It should be noted that the function $A = A(x, x_1, y, y_1, ...\omega, t_1, ...)$ appearing in equation (3.3) is different from the one in (3.4), where $A = A(x, x_1, ..., \kappa, \omega, t_1, ...)$. Since, however, both functions play the same role – an amplitude – in the derivation of the evolution equation, to keep the formulae simple we preferred to use the same notation for both.

Equation (3.4), valid for a mildly sloping beach all the way from deep into shallow water, is the starting point for the derivation of the stochastic model. It should be stressed that use is made of it in the following derivation only in the domain where the medium is still dispersive, that is beyond the region where Airy's theory for very long waves in shallow water is applicable (this is the 'semi-dispersive' domain of the model developed by Abreu *et al.* 1992 and requires special treatment). We shall first bring it to a discrete form, needed also for numerical integration purposes, by writing for the velocity potential the Fourier expansion

$$\phi = -\frac{\mathrm{i}}{2}\sum_{l=-\infty}^{\infty}\sum_{f=1}^{\infty}\left[A_{fl}\exp\left[\mathrm{i}\left(\int k_{x,fl}\mathrm{d}x + \kappa_l y - \omega_f t\right)\right]\right.$$
$$\left. -A^*_{fl}\exp\left[-\mathrm{i}\left(\int k_{x,fl}\mathrm{d}x + \kappa_l y - \omega_f t\right)\right]\right], \qquad (3.5)$$

which yields for the function φ the expression

$$\varphi = -\frac{\mathrm{i}}{2}(2\pi)^2 \sum_{l=-\infty}^{\infty}\sum_{f=1}^{\infty}\left[A_{fl}\exp\left(\mathrm{i}\int k_{x,fl}\mathrm{d}x\right)\delta(\omega+\omega_f)\delta(\kappa-\kappa_l)\right.$$
$$\left. -A^*_{fl}\exp\left(-\mathrm{i}\int k_{x,fl}\mathrm{d}x\right)\delta(\omega-\omega_f)\delta(\kappa+\kappa_l)\right],$$

with the mesh in the (ω,κ) domain defined as $\omega_f = f\omega_1$ and $\kappa_l = l\kappa_1$, $f = 1,2,\ldots$ (positive integer) and $l = \ldots,-2,1,0,1,2,\ldots$ (integer), and δ the Kronecker symbol. Substitution of the above into (3.4) gives the discrete equation

$$\frac{\partial A_{fl}}{\partial t_1} + \frac{1}{2}\frac{\partial}{\partial x}\left(C_{gx,fl}\right)A_{fl} + C_{gx,fl}\frac{\partial A_{fl}}{\partial x} + \mathrm{i}\left[\frac{g}{2\omega}(k_f^2-\sigma_f^4)\eta_0 + k_{x,fl}\frac{\partial\phi_0}{\partial x}\right]A_{fl}$$
$$= -\mathrm{i}\sum_{f_1,l_1}\sum_{f_2,l_2}\boldsymbol{W}_{(0,1,2)}A_{f_1l_1}A_{f_2l_2}\exp\left[-\mathrm{i}\int_{-\infty}^{x}\Delta_{0:1,2}\mathrm{d}x\right]\delta^{\omega}_{0:1,2}\delta^{\kappa}_{0:1,2}$$
$$-\mathrm{i}\sum_{f_1,l_1}\sum_{f_2,l_2}2\boldsymbol{W}_{(0,-1,2)}A_{f_1l_1}A_{f_2l_2}\exp\left[\mathrm{i}\int_{-\infty}^{x}\Delta_{2:0,1}\mathrm{d}x\right]\delta^{\omega}_{2:0,1}\delta^{\kappa}_{2:0,1}, \qquad (3.6a)$$

$$\boldsymbol{W}_{(0,\pm1,2)} = \frac{1}{8}\left[\pm 2\boldsymbol{k}_{f_1l_1}\cdot\boldsymbol{k}_{f_2l_2} + (\sigma_{f_1}\sigma_{f_2})^2 + k_{f_1}^2\frac{\sigma_{f_2}}{\sigma_f} \pm k_{f_2}^2\frac{\sigma_{f_1}}{\sigma_f} \mp \sigma_f^2\sigma_{f_1}\sigma_{f_2}\right], \qquad (3.6b)$$

where $C_{gx,fl} = C_{g,f}k_{x,fl}/k_f$ is the cross-shore component of the group velocity and $\Delta_{0:1,2} = k_{x,fl} - k_{x,f_1l_1} - k_{x,f_2l_2}$. By introducing the variable $B_{fl} = C^{1/2}_{gx,fl}A_{fl}$ one obtains, for the steady-state case, the somewhat simpler form

$$\frac{\mathrm{d}B_{fl}}{\mathrm{d}x} + \frac{\mathrm{i}}{C_{gx,fl}}\left[\frac{g}{2\omega_f}(k_f^2-\sigma_f^4)\eta_0 + k_f\phi_{0x_1}\right]B_{fl}$$
$$= -\mathrm{i}\sum_{f_1,l_1}\sum_{f_2,l_2}\widetilde{\boldsymbol{W}}_{(0,1,2)}B_{f_1l_1}B_{f_2l_2}\exp\left[-\mathrm{i}\int_{-\infty}^{x}\Delta_{0:1,2}\mathrm{d}x\right]\delta^{\omega}_{0:1,2}\delta^{\kappa}_{0:1,2}$$
$$-\mathrm{i}\sum_{f_1,l_1}\sum_{f_2,l_2}2\widetilde{\boldsymbol{W}}_{(0,-1,2)}B^*_{f_1l_1}B_{f_2l_2}\exp\left[\mathrm{i}\int_{-\infty}^{x}\Delta_{2:0,1}\mathrm{d}x\right]\delta^{\omega}_{2:0,1}\delta^{\kappa}_{2:0,1}, \qquad (3.7a)$$

$$\widetilde{\boldsymbol{W}}_{(0,\pm1,2)} = \boldsymbol{W}_{(0,\pm1,2)}\left(C_{gx,fl}C_{gx,f_1l_1}C_{gx,f_2l_2}\right)^{-1/2}. \qquad (3.7b)$$

A special modification of a rather standard procedure will be used in what follows to derive the stochastic model (see Sheremet 1996 for the details). Multiply equation (3.7) by B^*_{fl} and add to the complex conjugate of the same equation to obtain

$$\frac{\mathrm{d}|B_{fl}|^2}{\mathrm{d}x} = 2\sum_{f_1,l_1}\sum_{f_2,l_2}\widetilde{\boldsymbol{W}}_{(0,1,2)}\mathrm{Im}\left[B^*_{fl}B_{f_1l_1}B_{f_2l_2}\exp\left(-\mathrm{i}\int_{-\infty}^{x}\Delta_{0:1,2}\mathrm{d}x\right)\right]\delta^{\omega}_{0:1,2}\delta^{\kappa}_{0:1,2}$$
$$-2\sum_{k,f}2\widetilde{\boldsymbol{W}}_{(0,-1,2)}\mathrm{Im}\left[B^*_{fl}B^*_{f_1l_1}B_{f_2l_2}\exp\left(\mathrm{i}\int_{-\infty}^{x}\Delta_{2:0,1}\mathrm{d}x\right)\right]\delta^{\omega}_{2:0,1}\delta^{\kappa}_{2:0,1} \qquad (3.8)$$

where $\mathrm{Im}[F]$ denotes the imaginary part of F.

Under the common assumption that the modal phases are to leading order uncorrelated, the right-hand side of (3.8) cancels in the average yielding the linear approximation to the energy flux conservation equation. In order to obtain a description of the effect of the nonlinear interactions one has to go to higher-order terms, and

evaluate the derivative of products of the type $\partial(B^*BB)/\partial x$ using equation (3.7) and average again. Benney & Saffman (1966) have shown that for dispersive waves the leading-order contribution to the kinetic equation comes from products with repeated indices. Using the notation $\langle \ldots \rangle$ for the ensemble average one can write the relations

$$\frac{\mathrm{d}}{\mathrm{d}x}\langle B^*_{fl}B_{f_1l_1}B_{f_2l_2}\rangle = 2\mathrm{i}\left[\widetilde{W}_{(0,1,2)}\langle|B_{f_1l_1}|^2\rangle\langle|B_{f_2l_2}|^2\rangle + \widetilde{W}_{(1,-2,0)}\langle|B_{f_2l_2}|^2\rangle\langle|B_{fl}|^2\rangle + \widetilde{W}_{(2,-1,0)}\langle|B_{f_1l_1}|^2\rangle\langle|B_{fl}|^2\rangle\right]\exp\left[\mathrm{i}\int_{-\infty}^{x}\Delta_{0:1,2}\mathrm{d}x\right]\delta^{\omega}_{0:1,2}\delta^{\kappa}_{0:1,2}, \quad (3.9a)$$

$$\frac{\mathrm{d}}{\mathrm{d}x}\langle B^*_{fl}B^*_{f_1l_1}B_{f_2l_2}\rangle = -2\mathrm{i}\left[\widetilde{W}_{(0,-1,2)}\langle|B_{f_1l_1}|^2\rangle\langle|B_{f_2l_2}|^2\rangle + \widetilde{W}_{(1,-0,2)}\langle|B_{f_2l_2}|^2\rangle\langle|B_{fl}|^2\rangle + \widetilde{W}_{(2,1,0)}\langle|B_{f_1l_1}|^2\rangle\langle|B_{fl}|^2\rangle\right]\exp\left[-\mathrm{i}\int_{-\infty}^{x}\Delta_{2:0,1}\mathrm{d}x\right]\delta^{\omega}_{2:0,1}\delta^{\kappa}_{2:0,1}, \quad (3.9b)$$

which may be integrated with respect to x by assuming that the spectrum varies slowly with x. Integrating by parts, we may neglect the terms in which the derivatives of the spectrum appear, since they are $O(\epsilon^2)$ smaller. For simplicity we neglect the bispectrum in deep water (which is very small in a nearly Gaussian sea). It can be shown that this does not affect the shoaling spectrum.

After integration and substitution back into equation (3.8) one obtains the equation:

$$\begin{aligned}\frac{\mathrm{d}}{\mathrm{d}x}\langle|B_{fl}|^2\rangle = {} & 4\sum_{f_1,l_1}\sum_{f_2,l_2}[\widetilde{W}_{(0,1,2)}\langle|B_{f_1l_1}|^2\rangle\langle|B_{f_2l_2}|^2\rangle + \widetilde{W}_{(1,-2,0)}\langle|B_{f_2l_2}|^2\rangle\langle|B_{fl}|^2\rangle \\ & + \widetilde{W}_{(2,-1,0)}\langle|B_{f_1l_1}|^2\rangle\langle|B_{fl}|^2\rangle]\widetilde{W}_{(0,1,2)}\mathrm{Re}[\mathscr{J}_{0:1,2}]\delta^{\omega}_{0:1,2}\delta^{\kappa}_{0:1,2} \\ & + 8\sum_{f_1,l_1}\sum_{f_2,l_2}[\widetilde{W}_{(0,-1,2)}\langle|B_{f_1l_1}|^2\rangle\langle|B_{f_2l_2}|^2\rangle + \widetilde{W}_{(1,-0,2)}\langle|B_{f_2l_2}|^2\rangle\langle|B_{fl}|^2\rangle \\ & + \widetilde{W}_{(2,1,0)}\langle|B_{f_1l_1}|^2\rangle\langle|B_{fl}|^2\rangle]\widetilde{W}_{(0,-1,2)}\mathrm{Re}\left[\mathscr{J}_{2:0,1}\right]\delta^{\omega}_{2:0,1}\delta^{\kappa}_{2:0,1}. \end{aligned} \quad (3.10)$$

Here $\mathrm{Re}[F]$ means the real part of F. The function $\mathscr{J}$ appearing in (3.10) is defined as:

$$\mathscr{J}_{0:1,2} = \exp\left[-\mathrm{i}\int_{-\infty}^{x}\Delta_{0:1,2}\mathrm{d}x'\right]\int_{-\infty}^{x}\exp\left[\mathrm{i}\int_{-\infty}^{x'}\Delta_{0:1,2}\mathrm{d}\zeta\right]\mathrm{d}x'. \quad (3.11)$$

With a change of variables, we get

$$\mathscr{J}_{0:1,2} = \int_{-\infty}^{\infty}H(t)\exp\left[\mathrm{i}\int_{0}^{t}\Delta_{0:1,2}\mathrm{d}\zeta\right]\mathrm{d}t, \quad (3.12)$$

where H is the Heaviside function. $\mathscr{J}$ satisfies the simple differential equation

$$\frac{\mathrm{d}}{\mathrm{d}x}\mathscr{J}_{0:1,2} + \mathrm{i}\Delta_{0:1,2}\mathscr{J}_{0:1,2} = 1. \quad (3.13)$$

In (3.12) the dependence of $\mathscr{J}$ on x is by way of the argument of $\Delta_{0:1,2} = \Delta_{0:1,2}(x-\zeta)$. If the wavenumbers do not depend on the x-coordinate, as for the case of deep water, it may be seen from (3.12) that $\mathscr{J}$ is simply

$$\mathscr{J}_{0:1,2} = \pi\delta(\Delta_{0:1,2}) - \frac{\mathrm{i}}{\Delta_{0:1,2}}. \quad (3.14)$$

In the case of constant depth $\mathrm{Re}\left[\mathscr{J}_{0:1,2}\right] = 0$ and there is no triad interaction. For waves in which triad interaction is possible, the kernel for the interaction (which plays

a role similar to that of $\mathrm{Re}\left[\mathscr{J}_{0:1,2}\right]$), like the kernel for traditional four-wave interaction, is of a homogeneous medium, and the information of the global bathymetry does not enter the picture. In the case of an inhomogeneous medium, there is considerable build-up of the bispectrum (through the generation of large locked waves). The information about the bispectrum is implicitly brought in through the function $\mathscr{J}$, which stores the history of the bathymetry. Equation (3.10) can easily be generalized to include the term due to the initial bispectrum, when the sea is not initially Gaussian. We then see that this term gives rise to recurrence in the spectra of waves over a flat bottom.

The equation may also be written in terms of energy fluxes. Denote by F_{fl} the averaged linear energy flux corresponding to the Fourier mode (f, l), which is related to the former variable $\langle |B|^2 \rangle$ by

$$F_{fl} = \frac{1}{2}\frac{\omega_f^2}{g^2}\langle |B_{fl}|^2 \rangle \tag{3.15}$$

and the new form of the equation (3.10) is

$$\begin{aligned}\frac{\mathrm{d}}{\mathrm{d}x}F_{fl} = {} & 8\sum_{f_1,l_1}\sum_{f_2,l_2}\left[\boldsymbol{T}_{(0,1,2)}F_{f_1l_1}F_{f_2l_2} + \boldsymbol{T}_{(1,-2,0)}F_{f_2l_2}F_{fl} + \boldsymbol{T}_{(2,-1,0)}F_{f_1l_1}F_{fl}\right]\boldsymbol{T}_{(0,1,2)} \\ & \times \mathrm{Re}\left[\mathscr{J}_{0:1,2}\right]\delta^{\omega}_{0:1,2}\delta^{\kappa}_{0:1,2} \\ & +16\sum_{f_1,l_1}\sum_{f_2,l_2}\left[\boldsymbol{T}_{(0,-1,2)}F_{f_1l_1}F_{f_2l_2} + \boldsymbol{T}_{(1,-0,2)}F_{f_2l_2}F_{fl} + \boldsymbol{T}_{(2,1,0)}F_{f_1l_1}F_{fl}\right]\boldsymbol{T}_{(0,-1,2)} \\ & \times \mathrm{Re}\left[\mathscr{J}_{2:0,1}\right]\delta^{\omega}_{2:0,1}\delta^{\kappa}_{2:0,1},\end{aligned} \tag{3.16}$$

with the new kernel function $\boldsymbol{T}$ defined as

$$\boldsymbol{T}_{(0,\pm1,2)} = \frac{g\omega_f}{\omega_{f_1}\omega_{f_2}}\widetilde{\boldsymbol{W}}_{(0,\pm1,2)}. \tag{3.17}$$

Equation (3.16) is the main result of the present work. To integrate it numerically one needs only the power spectrum of the deep-water wave field and the beach bathymetry.

Both for reasons of simplicity and because of scarcity of data, preliminary testing of the stochastic directional shoaling model (3.16) has been conducted on the simplified unidirectional version that is obtained under the assumption that the waves propagate normally to the shore. For this particular case (3.16) reads

$$\begin{aligned}\frac{\mathrm{d}}{\mathrm{d}x}F_f = {} & 8\sum_{f_1,f_2}\left[\boldsymbol{T}_{0,1,2}F_{f_1}F_{f_2} + \boldsymbol{T}_{(1,-2,0)}F_{f_2}F_f + \boldsymbol{T}_{(2,-1,0)}F_{f_1}F_f\right]\boldsymbol{T}_{(0,1,2)} \\ & \times \mathrm{Re}\left[\mathscr{J}_{0:1,2}\right]\delta^{\omega}_{0:1,2} \\ & +16\sum_{f_1,f_2}\left[\boldsymbol{T}_{(0,-1,2)}F_{f_1}F_{f_2} + \boldsymbol{T}_{(1,-0,2)}F_{f_2}F_f + \boldsymbol{T}_{(2,1,0)}F_{f_1}F_f\right]\boldsymbol{T}_{(0,-1,2)} \\ & \times \mathrm{Re}\left[\mathscr{J}_{2:0,1}\right]\delta^{\omega}_{2:0,1}.\end{aligned} \tag{3.18}$$

Equations (3.18) and (3.13) form a closed system that may be integrated numerically given initial conditions in the form of a deep-sea power spectrum of the incoming wave field (since in this approximation the evolution of the wave field has no feedback from the evolution of the mean variables η_0 and ϕ_0 we shall ignore them in what follows).

An illustration of the idea used in the integration of (3.9) is given in figure 1(*a*)

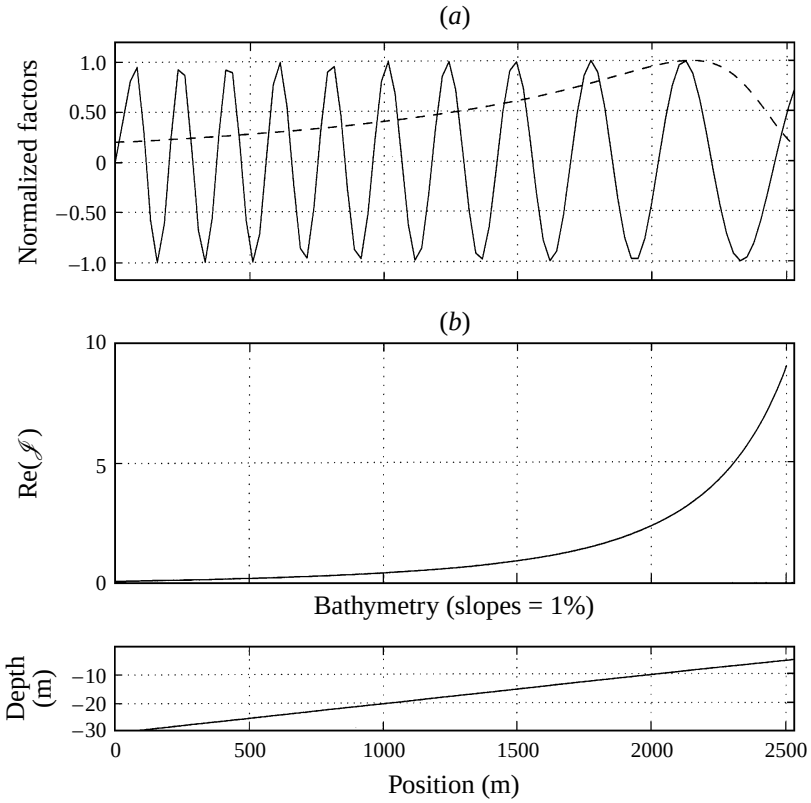

FIGURE 1. The evolution of the two factors in (3.9) plotted as functions of position for the peak and its second harmonic interaction (JONSWAP spectrum, ($T_{peak} = 12.2\,\mathrm{s}$, $H_{sig} = 2.2\,\mathrm{m}$)), shoaling over a 1% sloped bottom. (*a*) The term in the square brackets (dashed line) and the imaginary part of the exponential term (solid line). (*b*) The function $\mathscr{J}$ computed for the same triad.

where the evolution of the term in square brackets is plotted as a function of x for a typical spectrum (peak period 12 s – see §4.2). The interaction is of the triad $(f, f, 2f)$, f being the spectral peak frequency. The bottom slope is 1%. Also plotted is the imaginary part of the exponential term. It is seen that in this case the latter varies much faster than the former and we may 'take' the slowly varying term outside the integration. This scale separation is less pronounced in less dispersive situations (that is, larger Ursell parameter, see §4). Still, we find good agrreement with measurements and with the deterministic model. The evolution of $\mathscr{J}$ for the same triad is plotted in figure 1(*b*). It is seen that the spatial resolution required is largely reduced by not resolving the bispectrum.

Numerical examples using the simplified version of (3.18) are discussed in the next section.

4. Comparison with laboratory measurements

We have tested the performance of the numerical stochastic model against two sets of laboratory simulations: one for a bimodal spectrum evolution data from an experiment carried out by WES Research Division (a detailed presentation of the measurements is available in Briggs, Smith & Green 1991); and one for a more realistic unimodal shoaling spectrum (JONSWAP) from a set of measurements carried

out at CAMERI - Coastal and Marine Engineering Research Institute, Technion (for details see Sheremet & Stiassnie 1996).

Tests conducted on simulated data have shown that the number of modes chosen to describe the spectral evolution is not a critical parameter as long as the main features of the initial spectrum are preserved. The number of equations in the system grows roughly like N^2, where N is the number of Fourier modes, and although part of the equations (those for the $\mathscr{J}$ function) may be integrated separately, as they depend only on the bathymetry and the modal frequencies, the numerical effort can still be rather large. Therefore, the spectral analysis for the simulations was tuned to obtain smoother and lower-resolution spectral estimates, and the tail part of the spectrum was discarded (the energy in the discarded part was in both cases presented much less than 1% of the total energy). The number of modes was thus reduced to 30 for the bimodal simulations and 60 for the unimodal ones. In both cases, 50 independent runs were averaged to obtain the spectral evolution. Standard spectral analysis was used in both cases: each individual sequence was windowed using a Hanning window, then transformed to the frequency domain using standard FFT routines. The sample spectral densities were then averaged to obtain the power spectra.

The results of the stochastic numerical model were also compared to that of the averaged deterministic model derived by Agnon *et al.* (1993). We present the results of the runs only for one (the first) set of data, as reference – the deterministic model behaved consistently throughout. From measurements in time series form, the correct initial phases are readily derived; we note, however, that in general the initial data for such a model might well be expected to come from sources that give only spectral density information (an open-sea wave forecasting model for example).

To increase the readability of the numerical results, three frequency domains were separated by vertical lines: a 'long waves' a 'medium waves' and a 'short waves' band. The limits of each band were defined differently from case to case. It should be stressed that this division is done here in order to separate the spectral peaks. A 'band significant height' may be defined by the relation

$$H_{domain}^2 = 16 \int_{f_1}^{f_2} S(f)\mathrm{d}f \tag{4.1}$$

where *domain* stands for 'long', 'medium' or 'short' and f_1 and f_2 are the corresponding frequency limits. The above parameter may be regarded as a convenient way to describe the energy within a certain frequency interval.

As pointed out before, there is no sense in looking for a stochastic model for the case of unidirectional non-dispersive media. The usefulness of (3.18) depends on how close the actual data are to this case. One parameter that gives a measure of how close the case is to Airy's theory of very long waves in shallow water (non-dispersive medium) is the Ursell number $Ur = a/(k^2h^3)$ with a, k and h the characteristic amplitude and wavenumber of the wave field and the local depth respectively. The computed Ursell numbers (based on the 'band significant heights' and peak frequency) are given in the plots next to each of the peaks.

As a simple test of the statistical properties of the measurements, we compare the probability distribution of the normalized water level variable (zero mean and unit standard deviation) to the normal probability distribution, together with the evolution of the bicoherence. The natural evolution of the wave field during shoaling is quite obvious in both cases: the waves peak and develop longer and shallower troughs, in effect evolving towards a train of solitons. To obtain a measure of the modal phase

correlations we used the bispectral analysis techniques, e.g. Elgar & Guza (1985). The bispectrum is defined as the Fourier transform of the third-order cumulant:

$$\left.\begin{aligned}\mathscr{B}(\omega_1,\omega_2) &= \left(\frac{1}{2\pi}\right)^2 \int_{-\infty}^{\infty} \mathscr{S}(\tau_1,\tau_2)\exp\left[-\mathrm{i}\omega_1\tau_1 - \mathrm{i}\omega_2\tau_2\right]\mathrm{d}\tau_1\mathrm{d}\tau_2,\\ \mathscr{S}(\tau_1,\tau_2) &= \langle\eta(t)\eta(t+\tau_1)\eta(t+\tau_2)\rangle\end{aligned}\right\} \tag{4.2}$$

with $\mathscr{S}$ the third-order cumulant and the angular brackets the averaging operator. For discretely sampled data the digital bispectrum is

$$\mathscr{B}(\omega_k,\omega_j) = \langle A_{\omega_k} A_{\omega_j} A^*_{\omega_k+\omega_j}\rangle. \tag{4.3}$$

The bicoherence (the magnitude of the bispectrum normalized to the [0, 1] interval), which is a more convenient way to represent the phase correlation information, is defined by

$$b^2(\omega_k,\omega_j) = \frac{|\mathscr{B}(\omega_k,\omega_j)|^2}{\langle|A_{\omega_k}A_{\omega_j}|^2\rangle\langle|A_{\omega_k+\omega_j}|^2\rangle}. \tag{4.4}$$

For a Gaussian field the bicoherence is zero. The bicoherence will exhibit a pronounced peak at the frequencies (ω_k, ω_j) if the modes k and j are phase correlated.

4.1. *Bimodal spectral evolution*

From the laboratory data gathered by the WES Research Division (Briggs *et al.* 1991), the only case available to us that seemed to fit most of the restrictions imposed in the derivation of the model equation (3.18) – i.e. propagation normal to the shore over nearly parallel depth contours, with no breaking – was code named D81, a bimodal case with two peaks at the frequencies 0.4 and 0.8 Hz. The data consist of time series, 6500 records each (sampling frequency of 10 Hz) measured in an array of 20 locations of which 10 locations were distributed normally to the shore.

Figure 2 shows the evolution of the leading-order energy flux density (an invariant for a linear evolution). The plots indicate that the nonlinear evolution starts at about 26 cm depth, the fourth location in the cross-shore array. Breaking or other dissipation mechanisms appear to become active around the depth of 19 cm. We shall therefore omit the deeper locations in our presentation.

Figure 3 shows the probability distribution of the normalized water level against the normal distribution, together with the bicoherence at the same gauges. It seems that the Gaussian approximation is still valid only up to the depth of 29–25 cm. The evolution of the bicoherence given in figure 3 seems to confirm part of the expectations. Again, the sudden degradation of the correlations seen at the 15 cm depth indicates some dissipation.

The performance of the model (3.18) may be seen in figure 4 where the predicted power spectral density is plotted against the measured one. The predictions follow rather closely the measurements up to the depth of 15 cm. The results seem to indicate a value of Ur of about 1.5 as a possible threshold for the transition from a dispersive to non-dispersive medium.

Figure 5 shows the behaviour of the model derived by Agnon *et al.* (1993). The agreement with measurements is very good in the full range of depths, especially if we note that breaking begins at about 0.2 m depth. As noted above, in this region there is already dissipation of energy.

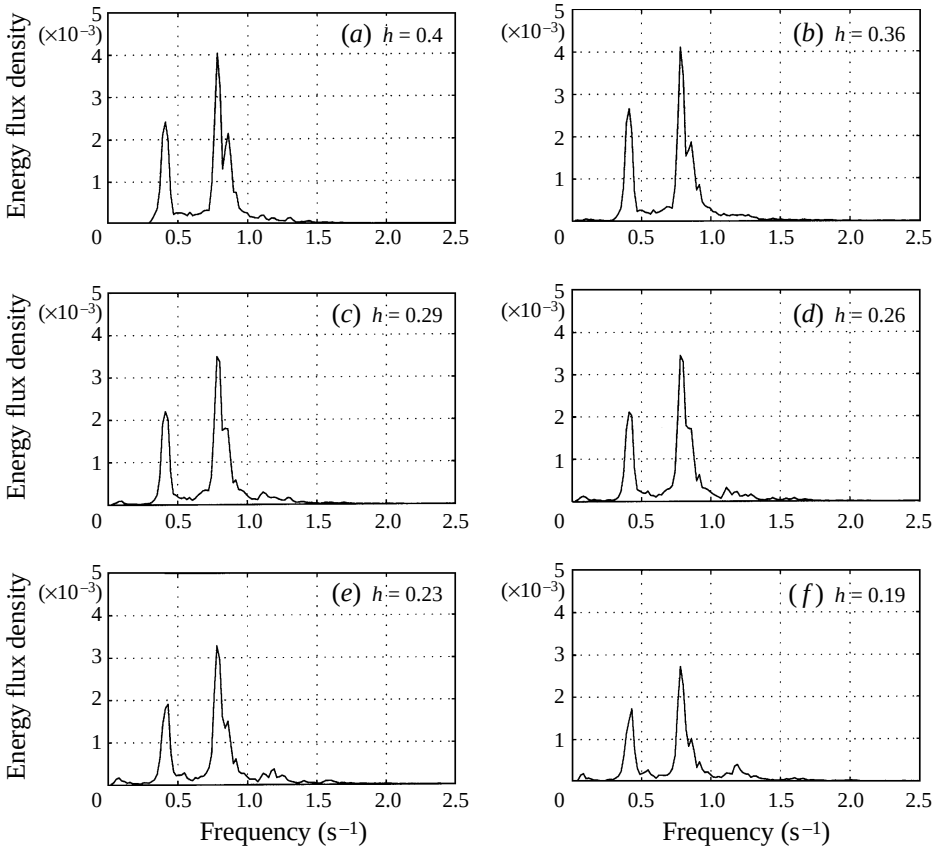

FIGURE 2. WES data set. Energy flux density evolution (*a–f*); the energy flux density is an invariant for linear shoaling.

4.2. *Unimodal spectrum (JONSWAP) simulations*

Being designed as simulations of typical storms in the Eastern Mediterranean, the CAMERI laboratory simulations (Sheremet & Stiassnie 1966) are, in a sense, a much more interesting testing ground for the present model. The experiment was carried out in the CAMERI towing tank, using a bi-dimensional model (scale 1:40) of the bathymetry in front of the Acre Harbour. The evolution of the waves was monitored from 30 m depth to 6 m depth (prototype), at 13 locations uniformly distributed along a region roughly divided into two segments: the first having a slope of about 5%, from 30 to 8 m depth, and the second with a slope of about 1%, from 8 to 6 m depth. Most of the nonlinear evolution occurred within the second shorter and shallower segment. A JONSWAP spectrum with $\gamma = 2.8$, characteristic of waves measured in the Eastern Mediterranean, was used to simulate the deep water spectral density. A total of 10 storm simulations with different peak periods and significant heights (ranging from 9 s to 14 s and from 1.5 m to 3 m respectively – care was taken to prevent wave-breaking) were performed with the aim to provide data for testing the stochastic model. The two cases we present ($T_{peak} = 12.2\,\mathrm{s}, H_{sig} = 2.2\,\mathrm{m}$) and ($T_{peak} = 14.4\,\mathrm{s},\ H_{sig} = 2.0\,\mathrm{m}$) are representative of the overall performance of the model.

All the numbers that appear in what follows refer to the prototype scale.

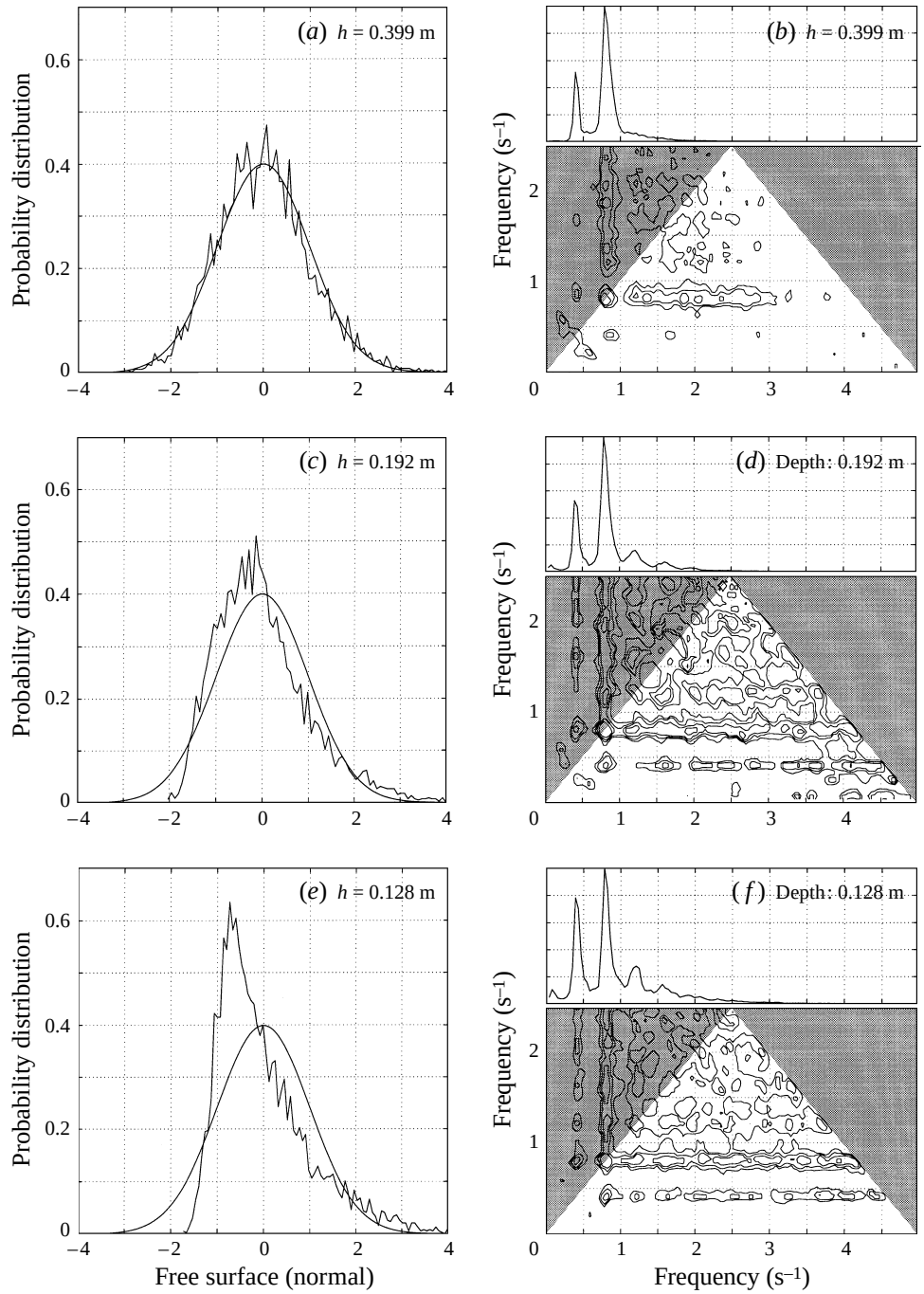

FIGURE 3. WES data set. Normalized time series histograms against the normal Gaussian distribution (a, c, e). The bicoherence at the same depths (b, d, f). The level curves are drawn at 0.2 increments.

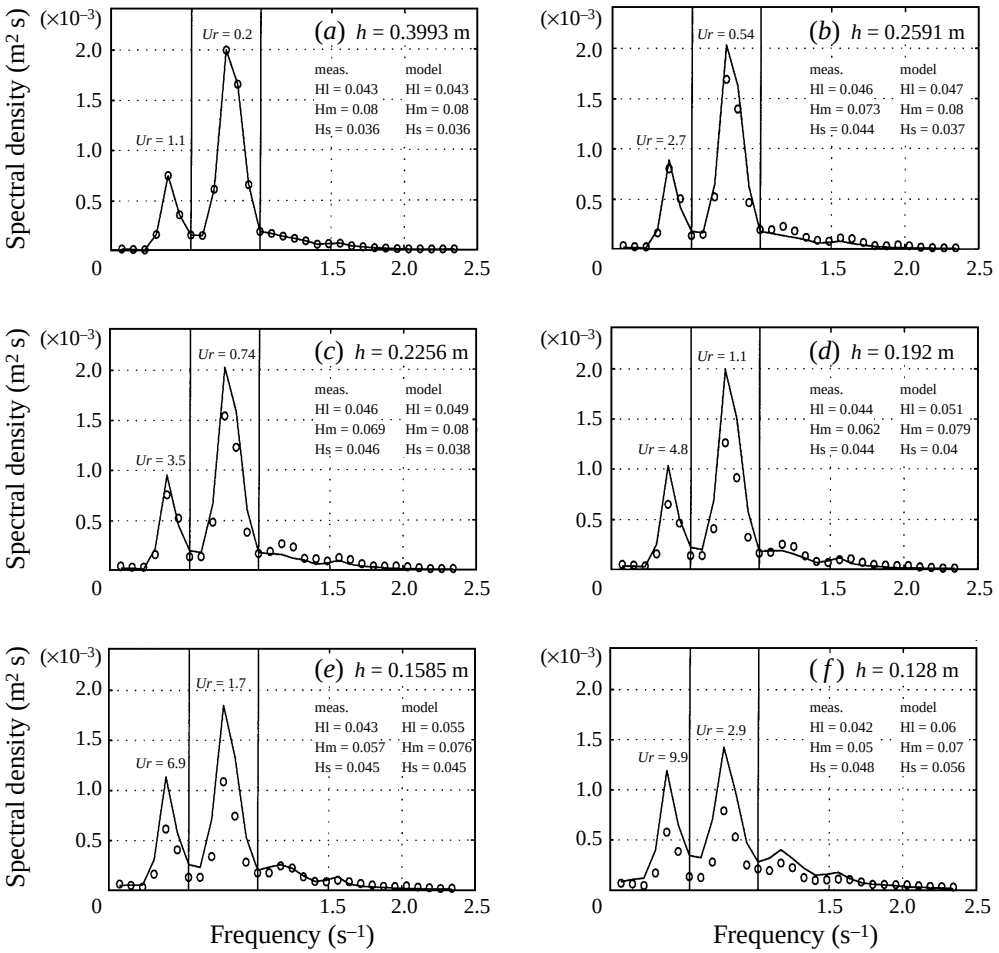

FIGURE 4. WES data set. Comparison of the numerical integration of the stochastic model (—) against measured data (○). The frequency domain is divided into three regions of 'long', 'medium' and 'short' waves. The computed 'significant height' (Hl, Hm, Hs for long, medium and short wave height) are shown for both the measured and the numerical solution. The corresponding Ursell number is written close to each of the spectral peaks.

As with the former case, we plot the evolution of the leading-order approximation to the energy flux density, in figure 6 for the case ($T_{peak} = 12.2\,\mathrm{s}, H_{sig} = 2.2\,\mathrm{m}$); little nonlinear evolution is observed up to gauge No. 8, at 9.6 m depth. The nonlinear energy transfer from the peak of the spectrum to its first and second harmonic is striking, as is the excitation of the longer waves in the spectrum.

The evolution of the bicoherence given in figure 7 for the same wave seems to confirm part of the expectations. The sea is Gaussian to a good approximation at the first gauge, at depth 30 m (prototype). While the spectral evolution is weak in the deeper segment of the domain, phase correlations are seen to build up, as the distribution of the sea surface becomes slightly skewed, with shallower and longer troughs and sharper peaks.

The performance of the stochastic model is shown in figures 8 and 9 for the ($T_{peak} = 12.2\,\mathrm{s}$, $H_{sig} = 2.2\,\mathrm{m}$) and ($T_{peak} = 14.4\,\mathrm{s}$, $H_{sig} = 2.0\,\mathrm{m}$) waves respectively. As before, we present the numerical spectra against the measured ones, plots (*a*) to (*e*). The

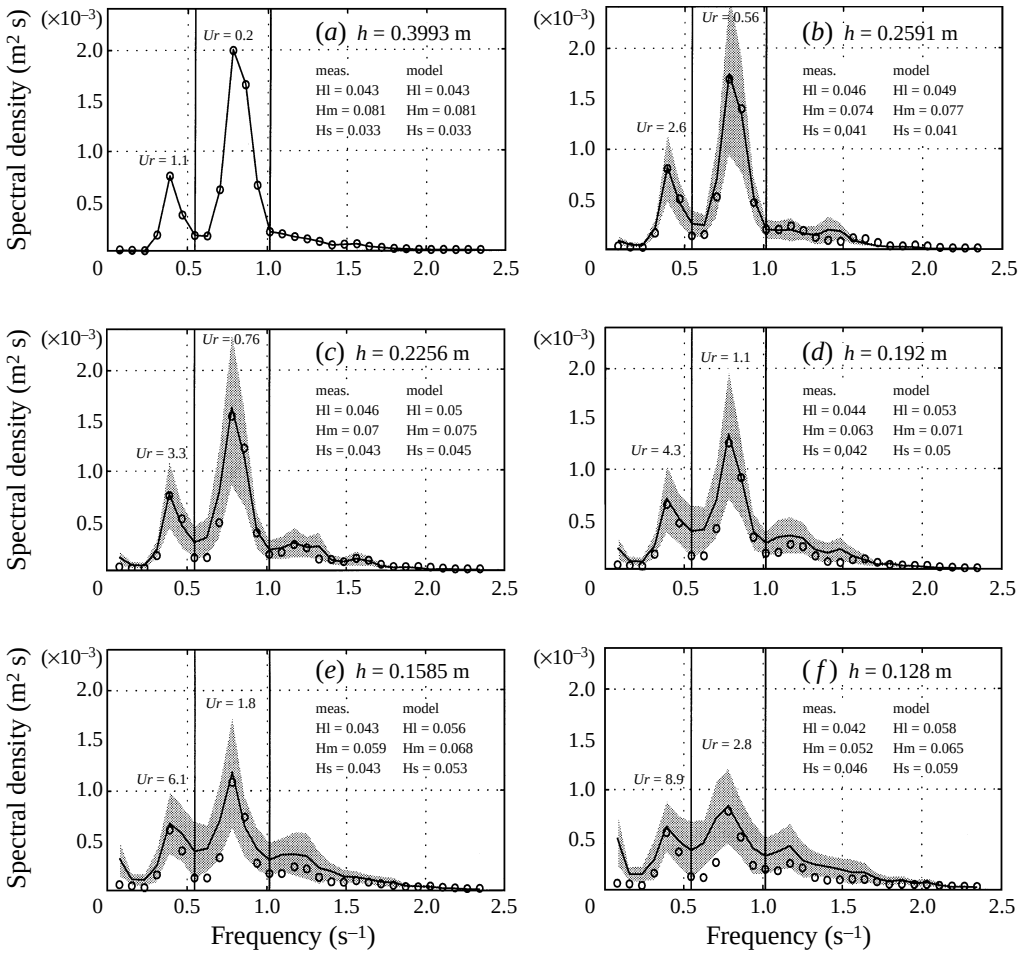

FIGURE 5. WES data set. Comparison of averaged numerical integrations of the deterministic model against measured data, power spectra (see figure 4 for notation). The phase sets were derived directly from fast-Fourier-transformed data sequences. The shaded area around the averaged numerical integrations has a vertical span equal to twice the standard deviation.

frequency domains separated by vertical lines are defined here by the 'long wave band' upper bound (at about 25 s) and the 'medium waves' one (at $\sim$9 s) which separate the spectral peak from its second harmonic. The Ursell number value is also written close to the spectral peak, along with the values of the 'band significant heights', measured and computed. One notices that the performance of the model is very good, again as long as the Ursell number stays smaller than 1.5, in agreement with the earlier observations. Figure 10 shows the evolution of the 'band significant heights' in the two cases presented. The model is seen to follow the trends of the measurements.

5. Conclusions

The unidirectional model of Agnon *et al.* (1993) may be generalized in a rather straightforward manner to a deterministic directional shoaling model for a non-breaking, edge-modes-free wave field over a mildly sloping beach. Imposing the addi-

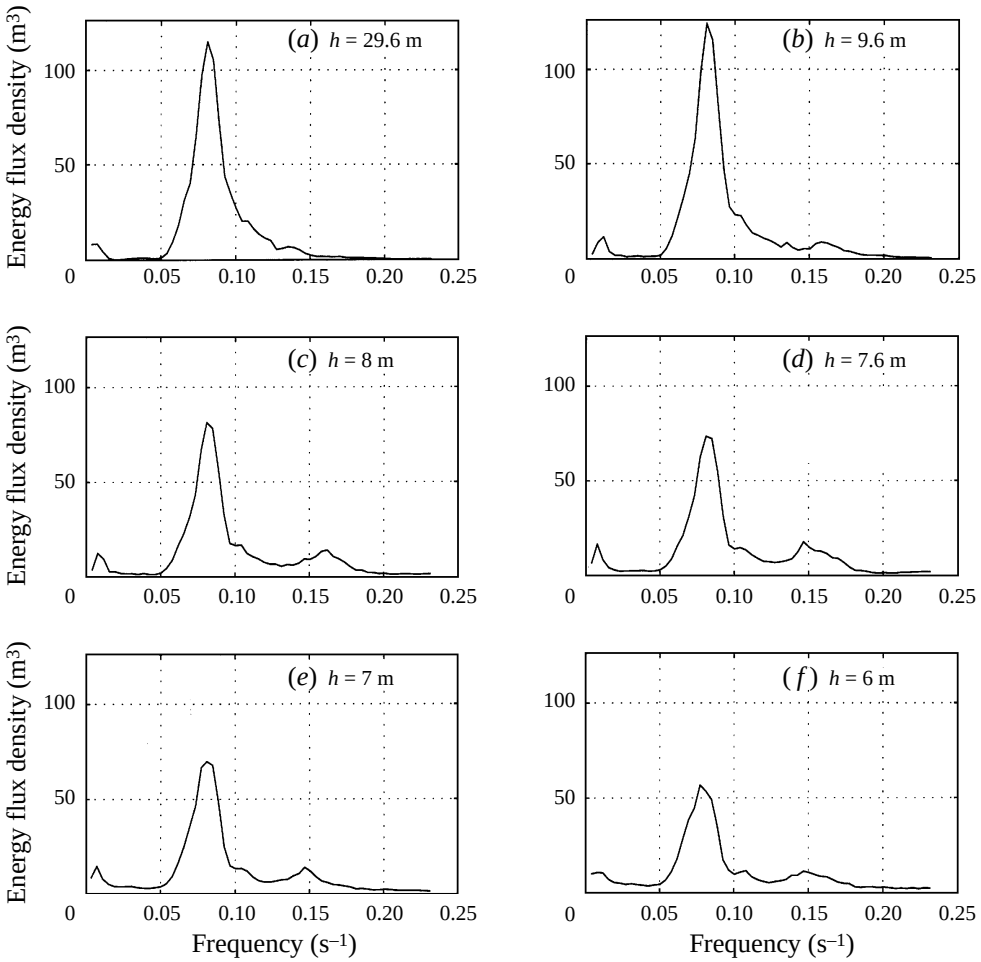

FIGURE 6. CAMERI data set ($T_{peak} = 12.2\,\text{s}$, $H_{sig} = 2.2\,\text{m}$). Energy flux density evolution, (a–f); the energy flux density is an invariant for linear shoaling.

tional restriction of parallel depth contours, the deterministic model may be averaged to obtain a stochastic directional shoaling model. The new stochastic model takes into account the development of phase correlation in bound waves in an implicit way. We see that in an inhomogeneous-medium non-resonant spectral evolution occurs.

Numerical simulations based on two sets of data are presented. The CAMERI data set is representative of the performance of the stochastic model throughout a rather extensive series of tests against laboratory data. The results of the numerical simulations agree well with the measurements, especially if one takes into account that the Acre bathymetry is not the ideal testing ground for the present model: 5% slope means a jump of 20 m in depth over a 400 m long stretch, barely twice the deep-water spectral peak wavelength, whereas the model was developed under the specific restriction of a mild bottom slope (say 1%). The model also lacks an energy dissipation mechanism – it cannot account for wave breaking, which might have occurred in the CERC experiment. However, it has been observed (Battjes & Beji 1992) that breaking does not change by much the shape of the spectrum. Indeed we see that the measured spectra are similar in shape to the calculated spectra, although their energy level is reduced.

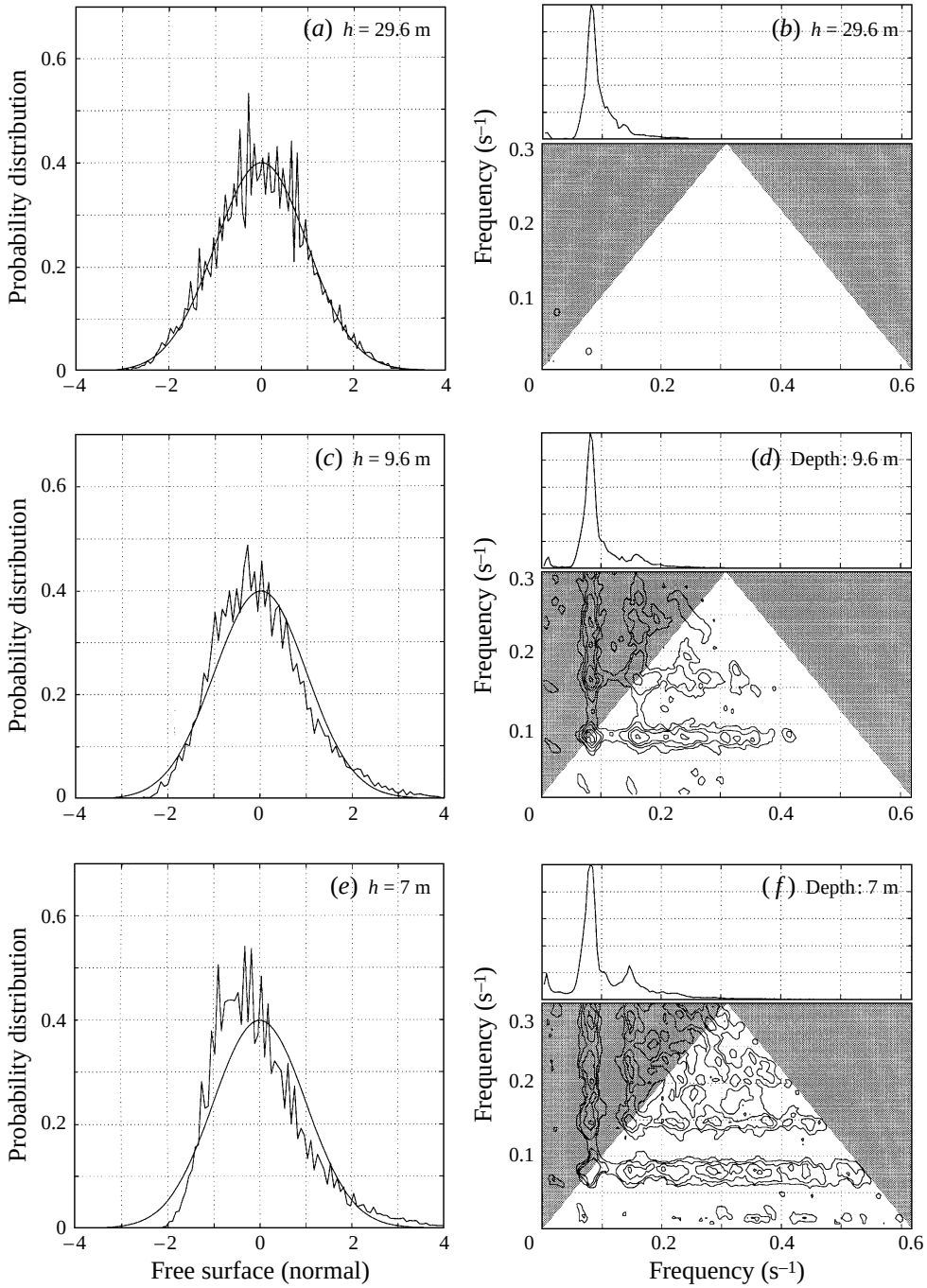

FIGURE 7. CAMERI data set ($T_{peak} = 12.2\,\mathrm{s}$, $H_{sig} = 2.2\,\mathrm{m}$). Normalized time series histograms against the normal Gaussian distribution (a, c, e). The bicoherence at the same depths (b, d, f). The level curves are drawn at 0.1 increments from the 0.3 level.

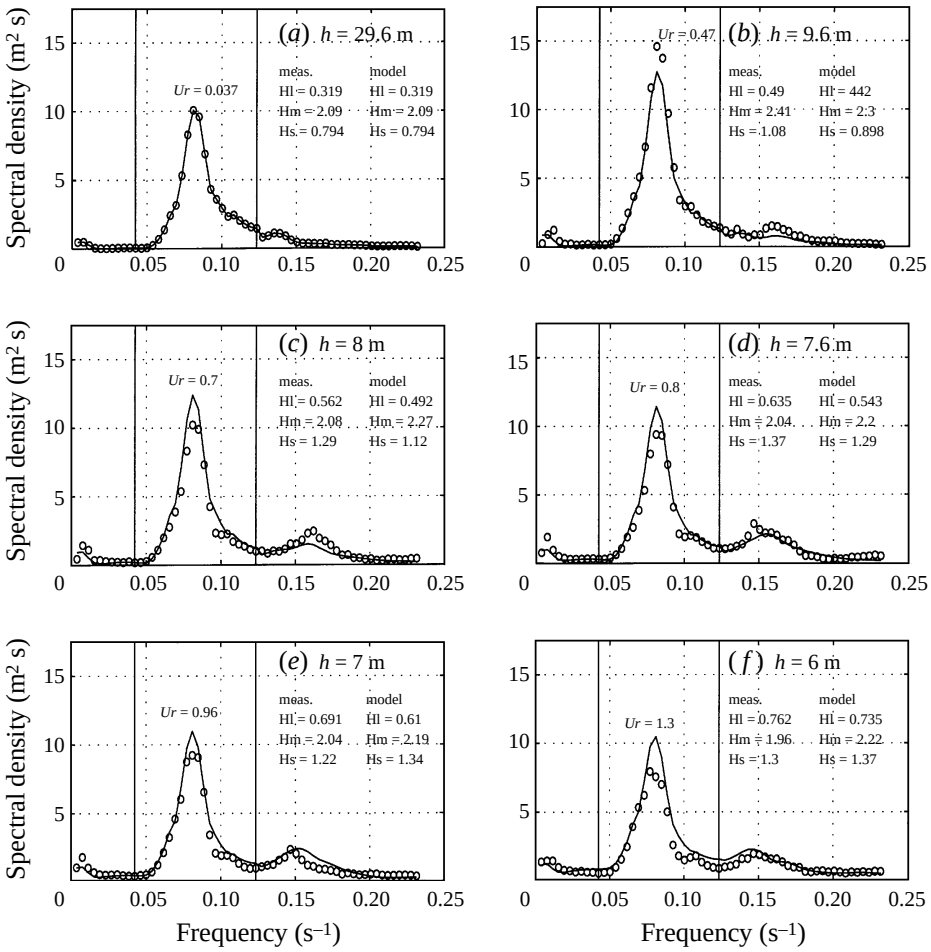

FIGURE 8. CAMERI data set ($T_{peak} = 12.2$ s, $H_{sig} = 2.2$ m). Comparison of the numerical integration of the stochastic model (—) against measured data (○) – see text and figure 4 for explanations.

Comparison with laboratory data seems to indicate that the model also works rather well beyond the domain where the waves may be regarded as Gaussian. The real limit of its usefulness is decided by the dispersivity of the medium. In a non-dispersive one-dimensional medium (very long waves in shallow water) there seems to be no possible closure and in this case unidirectional calculations lose all relevance (see the work of Abreu *et al.* 1992). Our numerical integrations appear to confirm these statements.

Good agreement with measurements was obtained for both the stochastic model and the averaged deterministic one, but it must be pointed out that although the former seems to solve the averaging problem, it does so under additional restrictions and assumptions. Given a sufficient number of realizations and the correct initial phases, the latter is, at least theoretically, better and valid in a wider domain. It is our feeling that the two should be regarded as complementary: for detailed analysis of an unknown sea state for which there is enough data and time, the deterministic approach should be chosen. However, routine forecasts that need speed and are

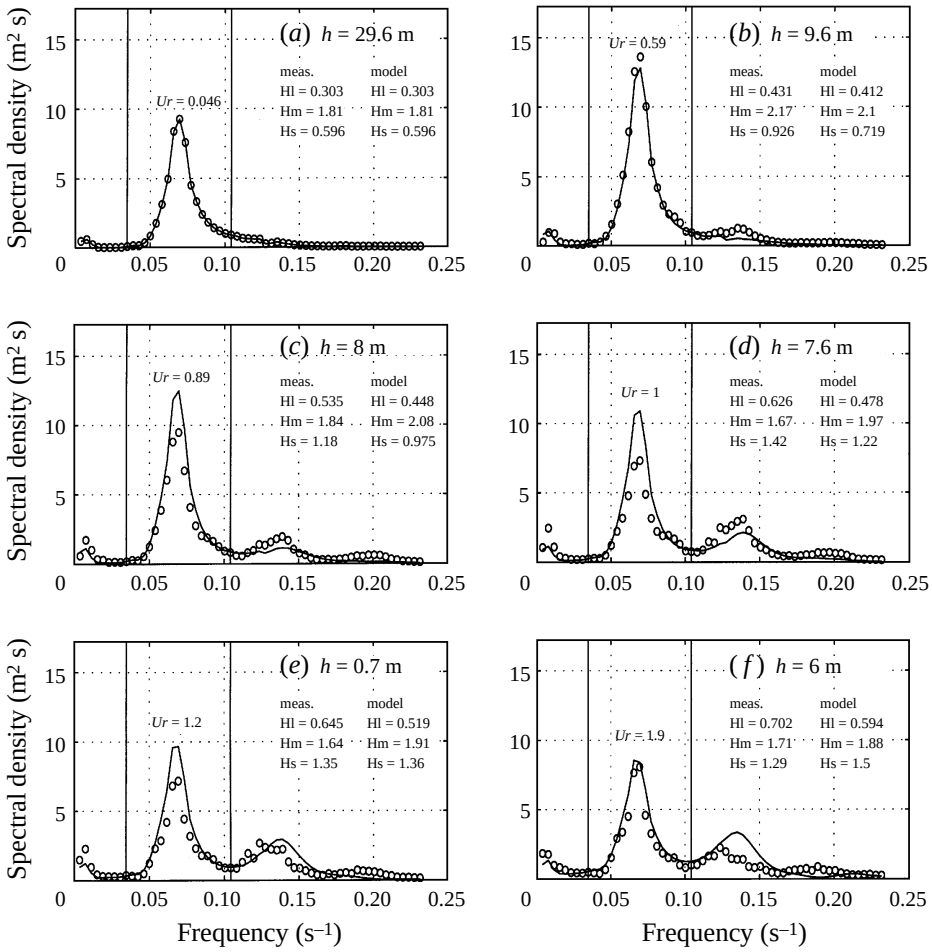

FIGURE 9. CAMERI data set, (T_{peak} = 14.4 s, H_{sig} = 2.0 m). Comparison of the numerical integration of the stochastic model (—) against measured data (○) – see text and figure 4 for explanations.

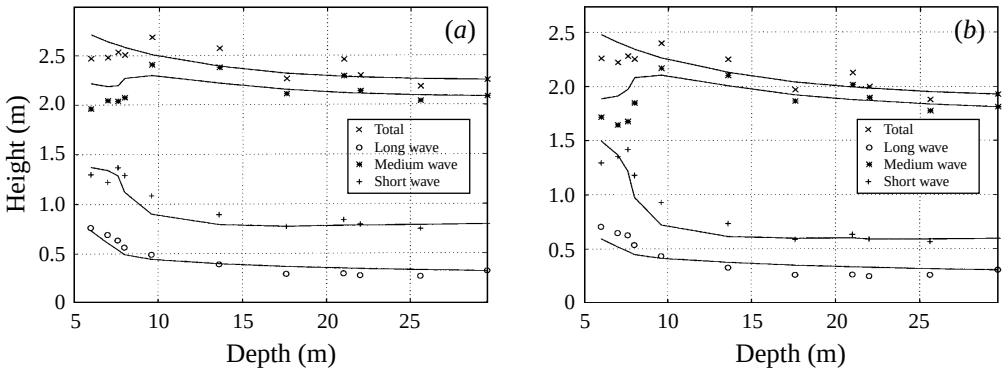

FIGURE 10. CAMERI data set. Evolution of the 'band significant heights' for the two cases presented in figures 8 and 9: (*a*) T_{peak} = 12.2 s, H_{sig} = 2.2 m and (*b*) T_{peak} = 14.4 s, H_{sig} = 2.0 m. Symbols are used to plot the measured data; the numerical integrations are plotted as solid lines.

dealing with sea conditions that are more or less understood are better served by stochastic models.

The present work is part of an ScD thesis by A. Sheremet submitted to the Department of Civil Engineering, Technion. We are grateful to Dr J. M. Briggs, Dr E. Thompson and Professor M. Stiassnie for providing data and comments, and to the referees for their discussions. This work was partly funded by the Danish National Research Foundation. Their support is greatly appreciated.

REFERENCES

Abreu, M., Larazza, A. & Thornton, E. 1992 Nonlinear transformation of directional wave spectra in shallow water. *J. Geophys. Res.* **97**, 15579–15589.

Agnon, Y., Sheremet, A., Gonsalves, J. & Stiassnie, M. 1993 A unidirectional model for shoaling gravity waves. *Coastal Engng* **20**, 29–58.

Battjes, J. A. & Beji, S. 1992 Breaking waves propagating over a shoal. *Proc. 23rd Intl Conf. on Coastal Engng* pp. 42–50. ASCE.

Benney, D. J. & Newell, A. C. 1969 Random waves closures. *Stud. Appl. Maths* **1**, 32–57.

Benney, D. J. & Saffman, P. G. 1966 Nonlinear interactions of random waves. *Proc. R. Soc. Lond.* A **289**, 301–321.

Briggs, M. J., Smith, J. M. & Green, R. D. 1991 Wave transformations over a generalized beach. *Tech. Rep. CERC-91-15 Wicksburg, Mississippi.*

Elgar, S. & Guza, R. T. 1985 Observations of bispectra of shoaling of surface gravity waves. *J. Fluid Mech.* **161**, 425–448.

Freilich, M. H. & Guza, R. T. 1984 Nonlinear effects on shoaling surface gravity waves. *Phil. Trans. R. Soc. Lond.* A**311**, 1–41.

Newell, A. C. & Aucoin, P. J. 1971 Semidispersive wave systems. *J. Fluid Mech.* **49**, 593–609.

Sheremet, A. 1996 Wave interaction in shallow water. ScD thesis, Technion, Haifa, Israel.

Sheremet, A. & Stiassnie, M. 1996 Laboratory validation of nonlinear shoaling computations. *ICZM in the Mediterranean & Black Sea, Proc. Intl Workshop, Sarigerme, Turkey*, pp. 391–403.

Suh, K. D., Dalrymple, R. A. & Kirby, J. T. 1990 An angular spectrum model for propagation of Stokes waves. *J. Fluid Mech.* **221**, 205–232.